Exp. Theo. NANOTECHNOLOGY 10 (2026) 1485-1499 https://doi.org/10.56053/10.3.1485

Experimental investigations of nano-Yttria (Y_2O_3) for electrochemical properties on Aluminum-based alloy

Shaimaa A. Naser[1], Noor Najm[2], Rand B. Lutfi[3], Rana A. Anaee[1,4,]*

[1]Nanotechnology and Advanced Materials Researches Center, University of Technology–Iraq, Baghdad, Iraq
[2]Petroleum and Gas Engineering Department, College of Engineering, University of Thi-Qar, Thi-Qar, Iraq
[3]Department of Physics, Collage of Education, Al-Iraqia University, Baghdad, Iraq
[4]College of Materials Engineering, University of Technology –Iraq, Baghdad, Iraq
*) Email: rana.a.majed@uotechnology.edu.iq

Received 25/3/2026, *Received in revised form* 13/4/2026, *Accepted* 25/6/2026, *Published* 15/7/2026

Sometimes aluminum composites have shown the properties better than their base alloys, therefore in this experimental research investigations three weight percent of nano yttria (Y_2O_3) are added to aluminum alloy with composition of Al-Si-Cu-Mg to study the corrosion behavior in simulated seawater. The characterization of the fabricated three composites is carried out by X-ray diffraction, scanning electron microscopy supported by energy dispersive spectroscopy and atomic force microscopy for three nano Y_2O_3% of 0.1, 0.3 and 0.5 weight percent. These three low percent are not detected in XRD, while the α-Al and Si with suggested phases Mg_2Si and Al_2Cu are appeared at their 2θ values. The inspection by FESEM/EDS gave indication to the presence of nano yttria particles within the alloy structure that lead to the clustering and rupturing the tree-like structure of the dendrite, this observation is supported by the increasing in W and O content by EDS analysis with increasing the added percent in fabricated composites. AFM analysis reflects the roughness of the composite's surface that related to appear cathodic and anodic sites, where the presence of the highest percent of nano yttria lead to increasing the cathodic area on the surface due to clustering the ceramic particles within metallic matrix. Electrochemical properties for fabricated composites compared with base alloy gave indication that the lowest addition is the best for corrosion resistance, where the corrosion current density is decreased by 1.5-6% for 0.1wt.% of nano yttria and all composites are shifted the corrosion

potential to the cathodic direction confirming the increasing of the cathodic area as well as the variation in the Tafel slopes that give indication for occurring different reactions on the surface.

Keywords: Nano yttria; Aluminum composites; Ceramic reinforcement; Tafel.

1. INTRODUCTION

Aluminum alloys take a wide range in their application to involve structural components especially in the automotive industries because of the high power-to-weight ratio, high wear resistance and low cost. Many elements are selected to be added to aluminum to form series of aluminum alloys that named as 2xxx, 3xxx, 4xxx, 5xxx, 6xxx and 7xxx according to the selected added element, followed by adding ceramic materials to form metal matrix composites (MMCs) for aluminum base. The applications of MMCs are different, for example in a diesel engine piston that prefer more than polymer matrix composites (PMCs) and ceramic matrix composites (CMCs) due to good mechanical properties. But still the corrosion or oxidation is the problematic issue. Many properties are offered by MMCs included thermal conductivity and lower thermal expansion, high stiffness and strength, and good wear resistance. In the field of the automotive industry, many requirements must be presented such as ecological and economical aspect, the construction of high-poared, comfortable and safe vehicles. Among Aluminum alloys, few of them contain Cu, Mg and Si are heat treatable in the casting technique because of the precipitation strengthening mechanisms. These alloys included the 3xxx series (casting aluminum alloys) and the 6xxx series (wrought aluminum alloys) that involve magnesium and silicon. The study of Al-Si-Cu/Mg alloys are done in many publications [1-3]. The microstructure of Al-Si-Cu-Mg alloy also studied with different Cu contents and Cu/Mg ratios to indicate that the Mg_2Si, θ-Al_2Cu and Q-type intermetallic phases will be formed [4]. To fabricate aluminum matrix composites, many oxides are selected as reinforcement, in 2013, three volume percent of magnesia (MgO) to reinforce aluminum that fabricate by melt-stirring for cutting tool uses [5], in 2014, three weight percent of yttria (Y_2O_3) are added to reinforce Al-Si-Cu alloy and the corrosion behavior is investigated in alkaline medium [6], in 2017, one weight percent of each graphene oxide (GO) and carbon nanotubes (CNTs) are selected to reinforce aluminum and the results showed the reducing in grain size with addition GO, but the poor dispersion with addition CNs [7], in 2017, 2 weight percent of MgO and 1 weight percent of SiC are added to reinforce Al-Ti alloy followed by heat treatment to indicate the formation of (Al_3Ti) and (Al_4C_3) from the decomposition of SiC as well as the produce of spinel ($MgO.Al_2O_3$) that enhance the corrosion resistance [8], nano iron oxide (Fe_2O_3) is added to reinforce aluminum by ultrasonic method to study the thermal behavior of produced metastable intermolecular composites and the results indicated that the micron size thermite gave an endothermic peak for Aluminum melting in DTA analysis [9], also various weight percent's of (MgO) is selected to reinforce AA7068 alloy by powder metallurgy technique to get improvement in wear resistance for produced composites [10], in 2018, different weight percent's of (α-Fe_2O_3) are added to reinforce aluminum and to study the thermal, magnetic and electrical properties, the results indicated the formation of FeAl phase through thermite reaction [11].

After 2020, the attempt to reinforce aluminum and its alloys remained continuous, where in 2021, the alumina (Al_2O_3) used to reinforce aluminum due to produced superior properties in aerospace industries, automotive industries and marine industries [12], also due to the good mechanical properties (tensile strength, hardness and high wear resistance) that associated with low weight and density [13], in 2022, different weight percent of (Al_2O_3) and (SiC) are selected to reinforce 7075 alloy and to improve the mechanical properties of base alloy in addition to use simulation study by Taguchi method and ANOVA technique [14], different weight percent of (α-Fe_2O_3, hematite) are added to improve mechanical properties and corrosion of aluminum that followed by heat treatments [15], while

in 2024, five weight percent of (Y_2O_3) are added to Aluminum-Al_2O_3 composites to improve the properties for solar thermal storage systems followed by compare the behavior with Al-12Si alloys as a microstructure, compatibility, thermophysical and mechanical properties [16].

In current experimental research work, three weight percent of nano yttria (Y_2O_3) are added to Al-Si-Cu-Mg alloy for investigate the microstructure changes and electrochemical properties in seawater medium at different temperatures.

2. EXPERIMENTAL

2.1. Materials

Al-Si-Cu-Mg alloy is fabricated by weighing the powder of these elements to add approximately silicon within (22-23 wt.%) and copper with magnesium within (≈ 1wt.%) and the remain as aluminum. To reinforce Al alloy, nano yttria (Y_2O_3) is added with three weight percents (0.1, 0.2 and 0.3) with grain size within (50-75 nm) by replacing the weight from aluminum. These materials are added in a special crucible and heating in an electrical furnace to about (700 °C) [17] with mixing at 300 rpm through 3 min to ensure of the dispersion of nano yttria particles within molten elements followed by the pouring of molten into a steel die to obtain a cylindrical specimen of each sample with diameter of 1.3 cm as rod of 0.5 cm in height. For inspection and corrosion measurements, these rods are cut, mounted, polished, and rinsed with acetone.

2.2. Inspections

To characterize the fabricated Al alloy-nano Y_2O_3 composites, many inspections are used involved the characterization of structural feature by X-ray diffraction (XRD) from (Shimadzu, $Japan$) at scanning rate of 1 degree.min^{-1} and the angular range is between 20° and 80°. To indicate the morphological feature, field emission scanning electron microscopy ($FESEM$) with (EDS) is used from (Thermo Fisher scientific company). While to indicate the topographical feature, atomic force microscope (AFM) is used from (NaioAFM 2022, Nanosurf, $Switzerland$).

2.3. Corrosion measurements

Electrochemical (Corrosion) measurements are achieved by potentiostat from Corrtest company (model: CS350M) with three known electrodes within special cell involved electrode to measure the potential by Calomel (Hg_2Cl_2/KCl) as $R.E$, to measure the current by Platinum (Pt) as $C.E.$, and the finally the samples of composites as $W.E$. Tafel plots are recorded for each sample and the data measured by applying Tafel extrapolation method to estimate corrosion potential (E_{corr}), corrosion current density (i_{corr}), and Tafel slope for cathodic section (b_c) and anodic other (b_a) at different temperatures [18, 19].

3. RESULTS AND DISCUSSION

3.1. The characterization of fabricated composites

Many techniques for characterization are used to show the change in structure, morphology and topography of fabricated Al alloy/Nano Yttria composites. The fist technique for characterization is X-ray diffraction from 20° to 80° for base alloy and three composites. Fig. 1 shows the patterns of all fabricated composites that indicate all peaks can be observed for Al-Si-Cu-Mg alloy as metal or phases

as illustrated by symbols in figure that included α-Al, Si, Mg_2Si phase and Al_2Cu phase, but no peak for yttrium can be seen in the patterns due to the weight percent's that less than (1 wt.%) [20, 21].

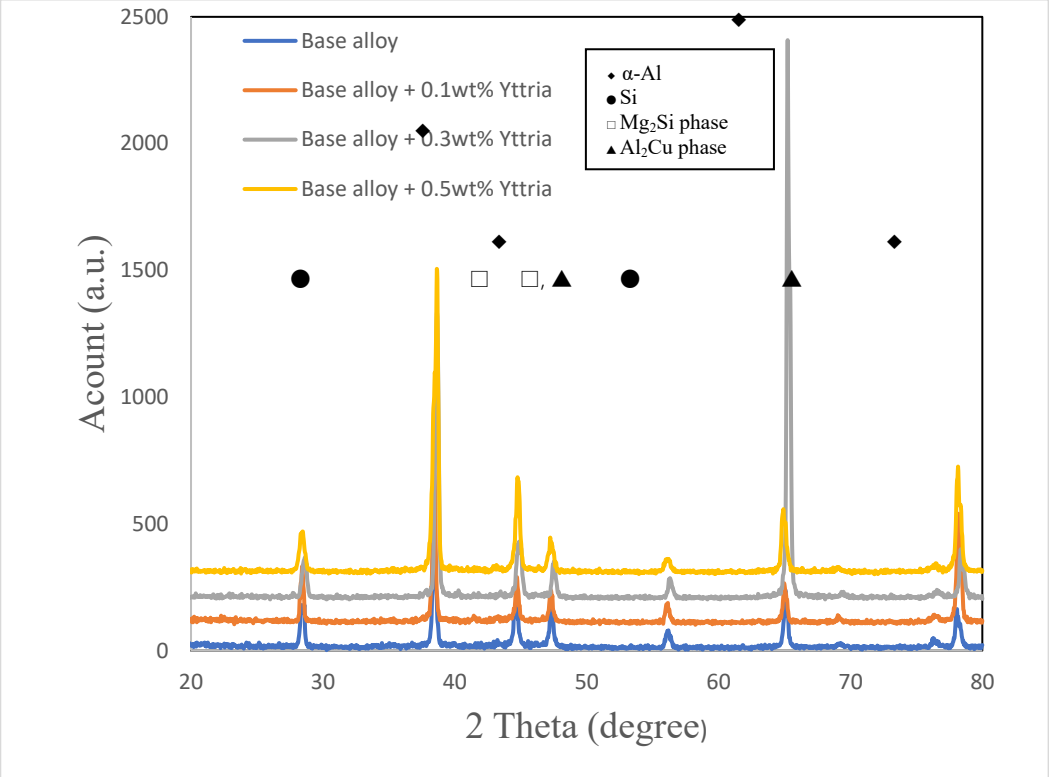

Figure 1 XRD pattern for fabricated composites.

The second technique for characterization is FESEM with EDS analysis, Fig. 2, a-d shows the FESEM images for fabricated composites. For base alloy, Al-Si-Cu-Mg alloy, the eutectic Si within the α-Al grain as a long strip is detected in addition to appear a small amount of Al_2Cu phase. Addition of nano yttria to base alloy decreases the formation of eutectic Si in the Al matrix due to clustering the added yttria in the way of a long strip of eutectic structure. The decreasing in the formation of eutectic structures increases with increasing the weight percent of nano yttria by 0.1, 0.3 and 0.5 % as shown in Fig. 2- b, c and d respectively. Finally, the presence of nano yttria particles within Al alloy matrix led to disorder in the main branch and arms of the dendrite feature that can get only the primary arm and reducing the arms of higher orders such as the secondary, tertiary and others. The EDS analysis in Fig. 3 that illustrates the weight percents of element content in the fabricated composites indicating the increasing of the oxygen and yttrium content with increasing the added yttria that confirm the presence of nano yttria within the Al-Si-Cu-Mg matrix.

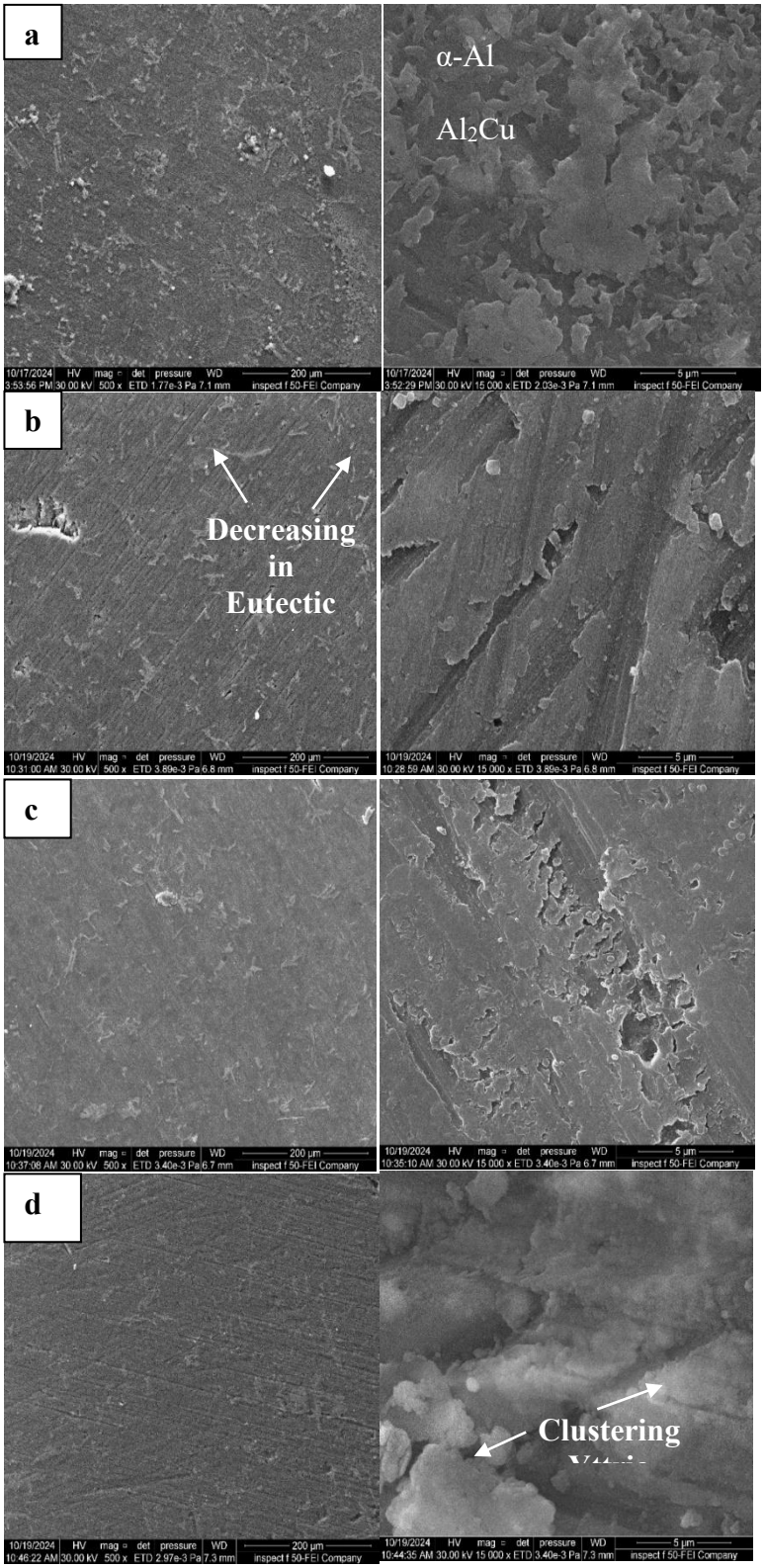

Figure 2 FESEM images for base alloy (a), Al alloy with 0.1wt.% yttria (b), Al alloy with 0.3wt.% yttria (c), and Al alloy with 0.5wt.% yttria (d).

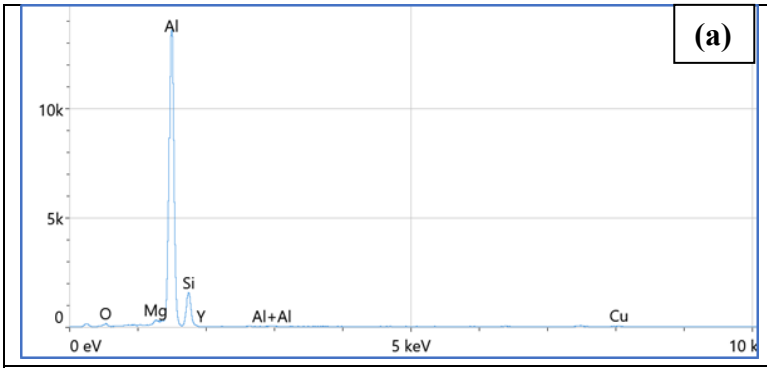

Element	Weight %
O	6.1
Mg	1.0
Al	68.4
Si	23.5
Cu	1.0
Y	0.0

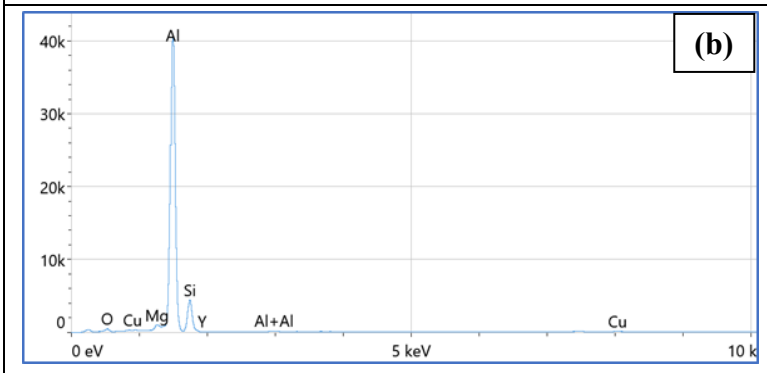

Element	Weight %
O	6.2
Mg	1.0
Al	68.7
Si	23.0
Cu	1.0
Y	0.1

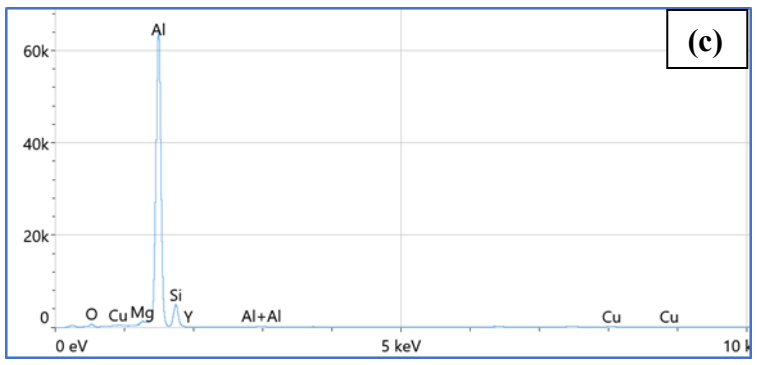

Element	Weight %
O	6.8
Mg	0.9
Al	68.5
Si	22.5
Cu	1.0
Y	0.3

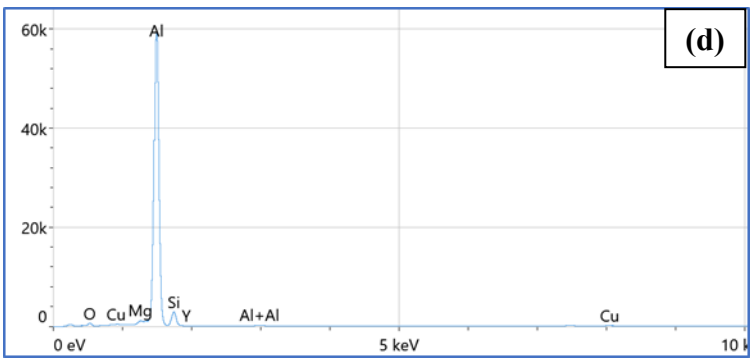

Element	Weight %
O	7.0
Mg	0.9
Al	68.6
Si	22.1
Cu	0.9
Y	0.5

Figure 3 EDS analysis for base alloy (a), Al alloy with 0.1wt.% yttria (b), Al alloy with 0.3wt.% yttria (c), and Al alloy with 0.5wt.% yttria (d).

AFM imaging gives a tool to topographical investigation through the two- and three-dimension view (Fig. 4, a – d) that indicate the feature of surface with the measuring of the surface roughness that related to formation of the galvanic cells in any electrolyte. These galvanic cells can be represented by the humps and valleys on the surface from the data of maximum height and depth that summary by root-mean-square height that listed in Table 1 to give the lowest value for base alloy (Al-Si-Cu-Mg), while the alloy/nano yttria composites have higher values that increase with the increasing of wt.% of yttria. The white blurry spots (humps) in Fig. 4, b – d refer to clustering the nano yttria particles. The mean height reflects the surface roughness for specimens which also gave the lowest value for base alloy and the higher values for composites that increase with the increasing of wt.% of nano yttria. Also, the number of particles on the surface took the same tendency followed by the mean dimeter due to presence of ceramic particles (Y_2O_3) within metals matrix that be clustered and segregated within eutectic structure and lead to rupture in the long strip of this structure.

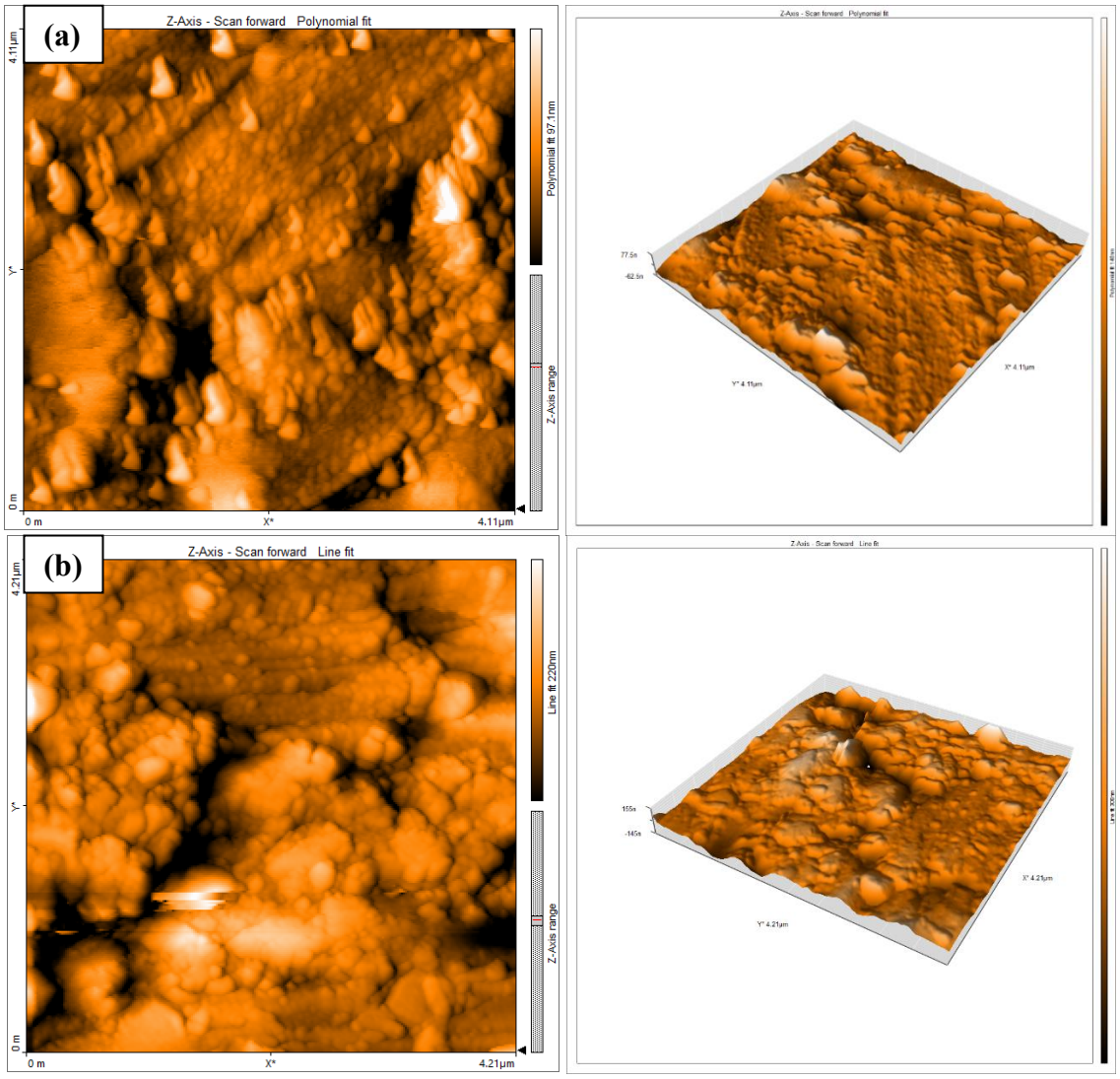

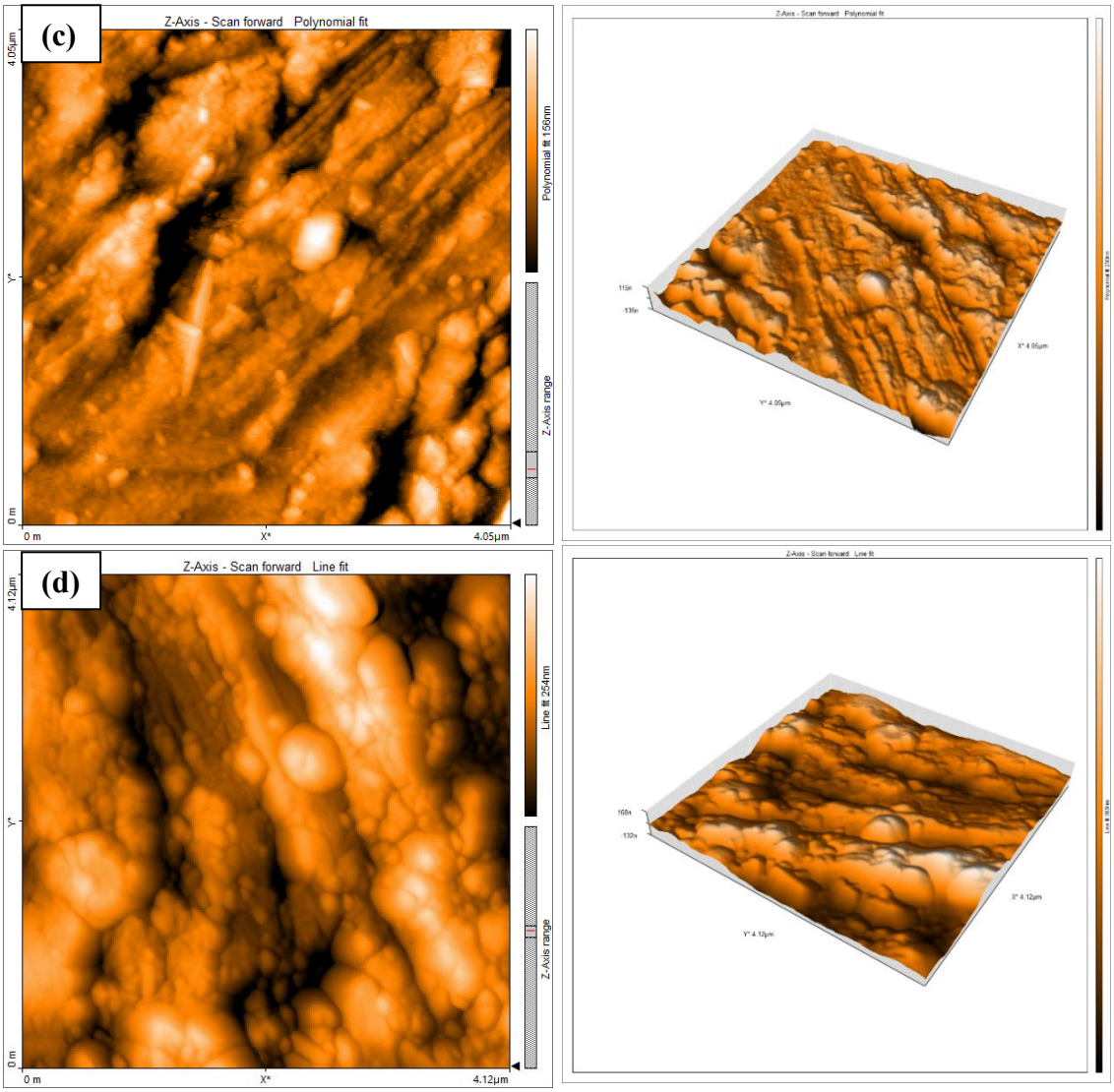

Figure 4 AFM images for base alloy (a) Al alloy with 0 wt.% yttria, (b) Al alloy with 0.1wt.% yttria, (c) and Al alloy with 0.3wt.% yttria, (d) and Al alloy with 0.5wt.% yttria.

Table 1 AFM data for fabricated specimens.

Y_2O_3wt.% in alloy	Root-mean-square height	Arithmetic mean height	No. of particles	Mean diameter
0	1.795 nm	1.523 nm	161	105.7
0.1	57.65 nm	42.98 nm	521	53.85
0.3	84.57 nm	60.44 nm	573	56.71
0.5	110.4 nm	80.35 nm	678	66.86

The changing in mean diameters on the Al alloy and fabricated composites surface is clear, it can be seen from histogram or distribution of the diameter as function to number of particles that refer to the mean diameter in base alloy is recorded as (105.7 nm) and is decreased after addition of the nano yttria

by ≈50% to be (53.85, 56.71 and 66,86 nm) for addition (0.1, 0.3 and 0.5 wt.%) of yttria respectively. This observation is clear from Fig. 5 in green columns related to small particle on the surface that give resistance compared with base alloy, but decreases among composites with increasing the clustering of the nano yttria in the matrix. During casting method, aluminum can convert to aluminum oxide by reaction with an atmosphere containing oxygen (O_2) and/or water moisture (H_2O) as the following reactions [22, 23]:

$$2Al + \frac{3}{2}O_2 \leftrightarrow Al_2O_3 \quad (1)$$

$$2Al + 3H_2O \leftrightarrow Al_2O_3 + 3H_2 \quad (2)$$

This amorphous film of oxide is unstable compared with its crystalline allotrope and may be transformed by nucleation and growth of a crystalline feature, also it may be η-Al_2O_3 or γ-Al_2O_3.

The addition of nano yttria can be led to the decreasing in mean diameter due to the significantly larger radius of yttrium ions (Y^{3+},0.093 nm) than the ionic radius of aluminum ions (Al^{3+}, 0.041 nm) which lead to cause the size difference followed by lattice distortion of (Al_2O_3) and creating stress fields that increase the defect deformation energy. Yttrium ions also create the numerous cationic vacancies in the alumina structure and promotes sintering that led to decreasing the alumina on the surface and remain the yttria at the grain boundaries, after that, the better compactness can occur between grains with fewer pores, and get increasing in the densification [16] which give the observed difference in mean diameters by AFM analysis.

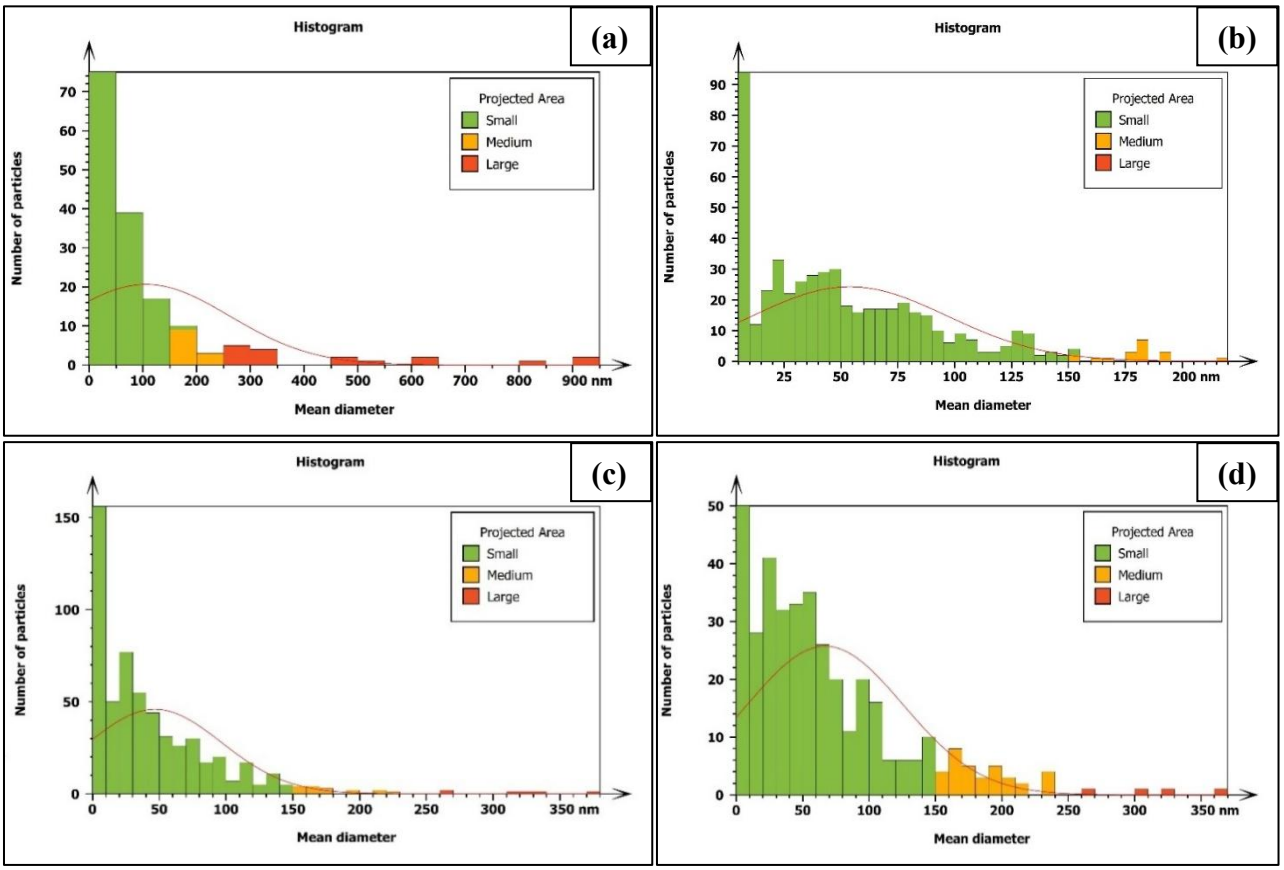

Figure 5 Histogram for base alloy (a) Al alloy with 0 wt.% yttria, (b) Al alloy with 0.1wt.% yttria, (c) and Al alloy with 0.3wt.% yttria, (d) and Al alloy with 0.5wt.% yttria.

3.2. Electrochemical properties

From the polarization curves (Figure 6) of Al alloy/Nano Y_2O_3 composites, can be seen that the corrosion potential always shifted to more active direction or cathodic direction due to increase the cathodic area compared with anodic once with different behavior with increasing wt.% of yttria addition. The tendency of corrosion current density is decreased for composites compared with the base Al alloy, but also with different behavior with increasing wt.% of yttria addition. It can be seen that the lowest percent (0.1 wt.%) has the lowest corrosion current density followed by (0.3 wt.%) and then (0.5 wt.%).

The corrosion behavior of aluminum base composites from the published literature is often contradictory because of the variety of the combinations between aluminum alloy matrices and reinforcement types. The composites in some cases are more susceptible to corrosion damage than the matrix alloy due to behave some reinforcements as cathodic area that increases the dissolution on anodic once. In seawater electrolyte, the Al alloy/nano yttria composites have polarization resistance (R_p) more than base Al alloy due to the role of yttria to enhancing the passive film of aluminum oxide (Table 2), this resistance is calculated according to the following formula [24-26]:

$$R_p = \frac{b_c \times b_a}{2.303 \times i_{corr} (b_c + b_a)} \quad (3)$$

The highest values of polarization resistance are recorded for composite with 0.1 wt.% nano yttria due to the role of yttria to reduce the diffusion of silicon atoms and decreases the wettability of the surface by the presence of ceramic coverage that lead to increasing the density of particles on the surface, where it is recorded the values of (22270234), (29387465) and (34849837) Particles/mm^2 for composites reinforced by 0.1, 0.3 and 0.5 wt.% yttria compared with the density of base alloy (9536233) Particles/mm^2 from AFM analysis. The decreasing of resistance with increasing wt.% of the nano yttria is due to creating a micro-galvanic coupling between the alloy matrix and yttria reinforcement and/or intermetallic phases that lead to damage of the protective oxide film because of the micro-segregation of the alloying elements and/or micro-crevices at the matrix/reinforcement interfaces.

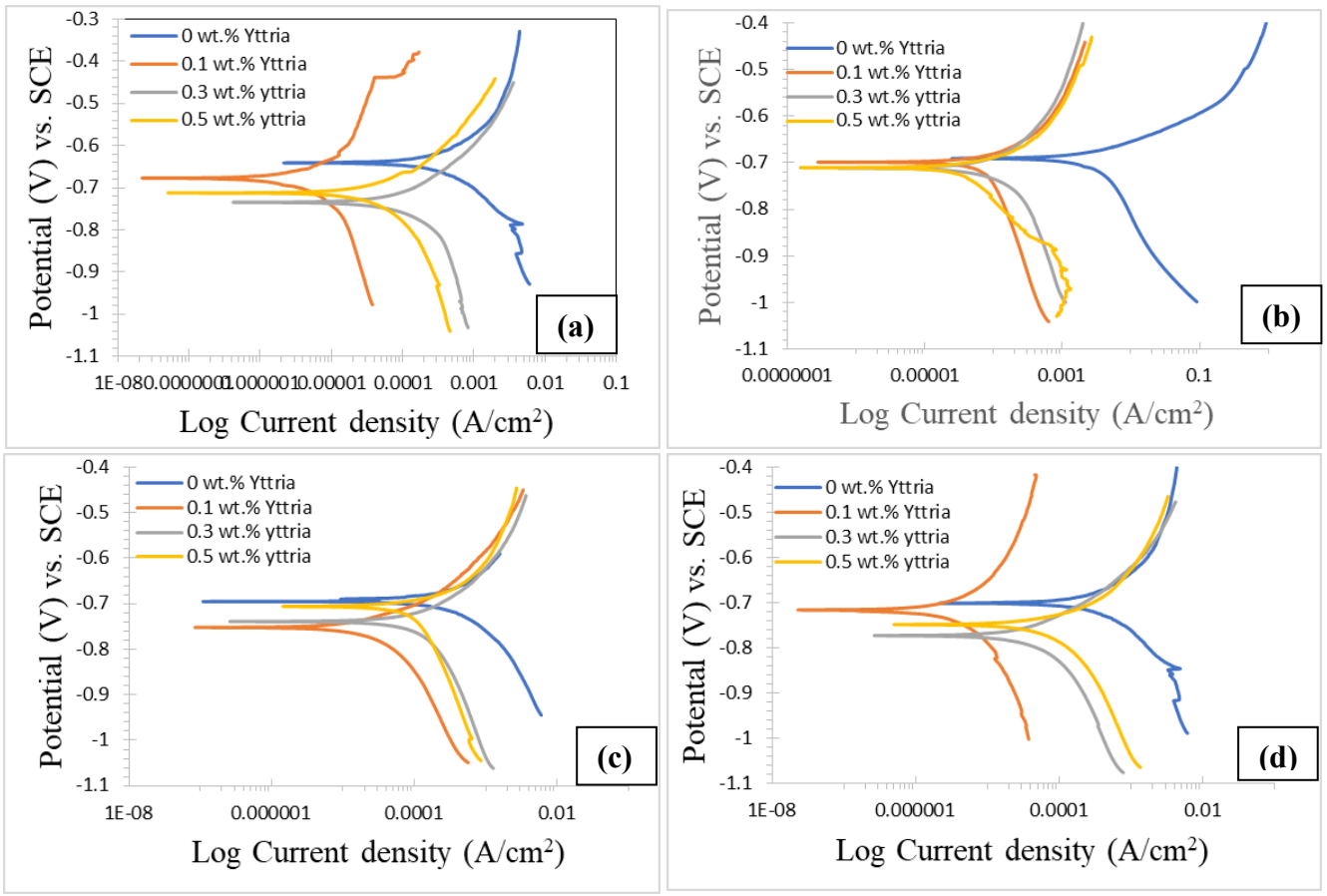

Figure 6 Tafel plots for base alloy and its composites at 298 K (a), 308 K(b), 318 K (c), and 328 K (d).

Table 2 Corrosion data of Al alloy/nano yttria composites in seawater at four temperatures.

Y_2O_3wt.% in alloy	Temp. (K)	$-E_{corr}$ (V)	$i_{corr}\times10^{-5}$ ($A.cm^{-2}$)	$-b_c$ ($mV.dec^{-1}$)	$+b_a$ ($mV.dec^{-1}$)	$R_p\times10^2$ ($\Omega.cm^2$)
0	298	0.642	35.25	160.62	199.61	1.096
	308	0.692	37.13	236.75	62.497	0.578
	318	0.695	50.27	368.69	53.386	0.402
	328	0.718	65.95	457.81	60.44	0.351
0.1	298	0.677	0.560	94.394	64.386	29.67
	308	0.699	2.091	483.13	81.895	14.54
	318	0.752	3.135	446.95	78.304	9.228
	328	0.717	4.157	61.976	56.294	3.081
0.3	298	0.734	1.127	43.554	34.995	7.476
	308	0.711	3.009	98.398	90.799	6.814
	318	0.739	4.504	214.41	100.17	6.582
	328	0.773	6.865	250.27	130.91	5.436
0.5	298	0.712	3.442	572.31	21.46	2.609
	308	0.710	4.229	119.97	29.348	2.421
	318	0.706	5.561	38.894	40.834	1.555
	328	0.748	7.089	23.784	95.155	1.165

3.3. Kinetic and thermodynamic of corrosion

The kinetic of corrosion can estimated respect to a temperature by Arrhenius equation as shown below and illustrated in Fig. 7 [27]

$$i_{corr} = A \,.\, e^{-E_a/RT} \quad (4)$$

where A and E_a are referred to the pre-exponential factor and activation energy of the corrosion respectively. The activation energy values are estimated from the slope of each relationship that recorded (7.647 kJ/mol) for Al alloy, while get (22.876, 20.671 and 8.603 kJ/mol) for composites with 0.1, 0.3 and 0.5 wt.% yttria respectively. The highest activation energy is for composite with 1wt.% yttria that refer to the needing the most energy to corrosion occur for surmount the energy barrier.

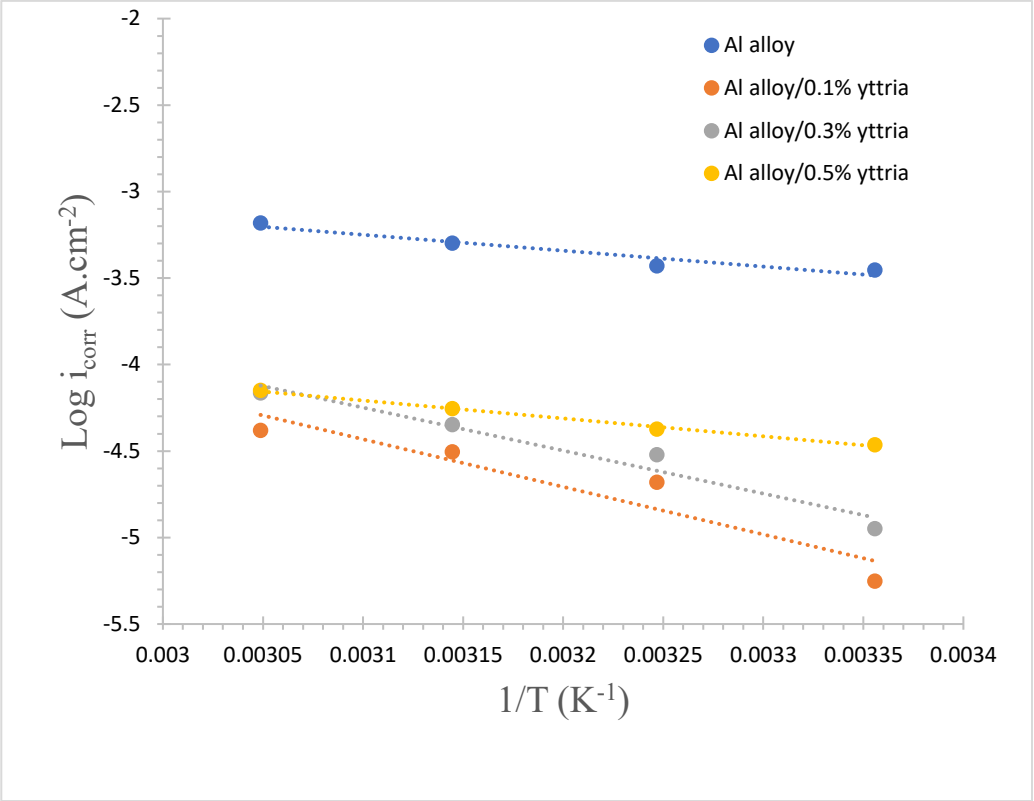

Figure 7 Arrhenius relation for fabricated composites.

Thermodynamics calculations are widely applied for corrosion of composites that include the change in the Gibbs free energy (ΔG) which reflect the work capacity presented in the system to the reactions of Corrosion/Dissolution that occurs at electrodes through the relation [28];

$$\Delta G = -nFE_{corr} \quad (5)$$

where n refer to number of electrons in the reaction that equal to (3) and F mean Faraday constant which equal to (96 485 C/mole). The change in free energy gave near negative values for all specimens that tell us with the strong tendency transform of high energy state of particles (Atoms and molecules) to low energy state (Corrosion products). This change in free energy has relation with temperature to estimate the change in the entropy which has a quantity of (ΔS) as follow [29];

$$\Delta S = -\frac{d(\Delta G)}{dT} \quad (6)$$

This relation can be illustrated in Fig. 8 that has a slope equal to the change in entropy, where this magnitude refers to the change in the order and/or orientation of the species in system of corrosion such as dissolved oxygen to be reduce at cathodic sites, metal atoms to be oxidized at anodic sites and water molecules to form the hydrated or solvated metal ions at the electrical double layer. The values of the change in entropy (ΔS) have positive sign because of negative sign of the change in energy as listed in Table 3, the entropy of corrosion in initial stage is constant which refer to (S_1), while the entropy or disorder is varied for final stage (S_2), i.e., at electrical double layer. This change can be expressed as [30, 31];

$$\Delta S = S_2 - S_1 \quad (7)$$

The change in entropy for composites are lower than for base Al alloy, and decreased with increasing the wt.% of nano yttria due to decreasing in the disorder of the species at the double layer because of enhancing the passive layer of aluminum oxide by yttrium oxide, i.e., the decreasing in S_2 with increasing wt.% of yttria compared with the S_1 that reflect the state of metallic atoms within the lattice structure [32, 33].

These two thermodynamic functions (ΔG) and (ΔS) are related to the other function refer to the change in enthalpy (ΔH) according to the following equation

$$\Delta G = \Delta H - T\Delta S \quad (8)$$

This change (Enthalpy) is related to the reaction nature which occur especially the oxidation or dissolution and has two signs; the positive which reflect the endothermic and negative which reflect exothermic nature and also included some effects as follow [30, 31]:

$$\Delta H = S + I_M - W_{M^{n+}} - (\frac{1}{2}D_{H_2} + I_H - W_{H^+}) \quad (9)$$

where S represent the heat of sublimation for the metal (Al), I_M represent the ionization potential of the metal (Al^{3+}), $W_{M^{n+}}$ represent the heat hydration of the metal ions in the environment, D_{H_2} represent the bond-dissociation energy of (H_2), I_H represent the ionization potential of (H) and W_{H^+} represent the heat of (H^+) [37, 38].

By neglecting the right constant part $(\frac{1}{2}D_{H_2} + I_H - W_{H^+})$, it can be seen that the change in enthalpy for fabricated specimens is related to the following [39-41]:

$$\Delta H = S + I_M - W_{M^{n+}} \quad (10)$$

These three parameters are different for metallic alloys compared with metal matrix composites [42,43].

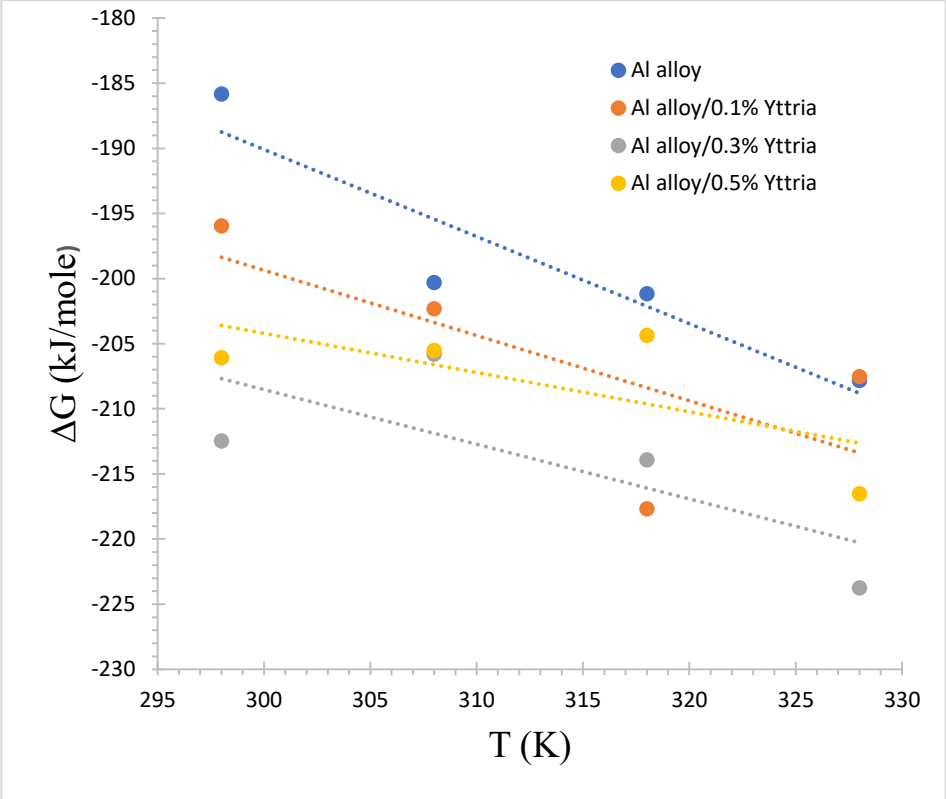

Figure 8 The variation of ΔG with temperature for fabricated specimens.

Table 3 Thermodynamic data of Al alloy/nano yttria composites at four temperatures.

Y_2O_3wt.% in alloy	Temp. (K)	-ΔG (kJ/mole)	ΔS (kJ/mole.K)	ΔH (kJ/mole)
0	298	-185.830	0.66864	13.412
	308	-200.303		5.625
	318	-201.171		11.443
	328	-207.829		11.472
0.1	298	-195.961	0.50076	-46.734
	308	-202.329		-48.095
	318	-217.670		-58.428
	328	-207.539		-43.290
0.3	298	-212.460	0.41971	-87.389
	308	-205.803		-76.534
	318	-213.907		-80.442
	328	-223.749		-86.087
0.5	298	-206.092	0.30103	-116.38
	308	-205.513		-112.796
	318	-204.355		-108.628
	328	-216.512		-117.775

4. CONCLUSIONS

Nano yttria as ceramic particles were added to aluminum alloy with three low eight percents (0.1, 0.3 and 0.5) to investigate the corrosion behavior. The added percent were improved the resistance, but remine the lowest percent was the best due the clustering of particles that occur when added higher percent because of the different between the structure of metals and ceramics. Many techniques were used to characterization such as XRD that did not give indication about addition due to low percents, SEM/EDS that show the role of yttria addition through rupture the arms of eutectic structures and AFM that gave indication for topographies through roughness and mean diameters. Some calculations in the corrosion branch were achieved.

References

[1] M. A. M. A. Mohamed, F. H. Samuel, S. Alkahtani, Materials Science and Engineering A, 543 (2012) 22. https://doi.org/10.1016/j.msea.2012.02.084
[2] M. A. M. A. Mohamed, A. M. Samuel, F. H. Samuel, H. W. Doty, Materials & Design, 30 (2009) 3943. https://doi.org/10.1016/j.matdes.2009.05.042
[3] M. Djurdjevic, T. Stockwell, J. Sokolowski, International Journal of Cast Metals Research, 12 (1999) 67. https://doi.org/10.1080/13640461.1999.11819209
[4] Y. Zheng, W. Xiao, S. Ge, W. Zhao, S. Hanada, C. Ma, Journal of Alloys and Compounds, 649 (2015) 291. https://doi.org/10.1016/j.jallcom.2015.07.090
[5] M. Pul, G. Uzun, R. Çalın, U. Şeker, Science and Engineering of Composite Materials, 20 (2013) 155. https://doi.org/10.1515/secm-2012-0034
[6] R. A. Anaee, Asian Journal of Chemistry, 26 (2014) 4469. https://doi.org/10.14233/ajchem.2014.17005
[7] P. Hidalgo-Manrique, S. Yan, F. Lin, Q. Hong, I. A. Kinloch, X. Chen, R. J. Young, X. Zhang, S. Dai, Journal of Materials Science, 52 (2017) 13466. https://doi.org/10.1007/s10853-017-1434-4
[8] R. A. Anaee, W. M. Salih, B. F. Dawood, Journal of Bio- and Tribo-Corrosion, 3 (2017) 38. https://doi.org/10.1007/s40735-017-0098-8
[9] F. Boudou, A. Belakredar, A. Berkane, M. RASHEED, Notulae Scientia Biologicae, 17 (2025) 12183. https://doi.org/10.55779/nsb17212183
[10] K. J. Joshua, S. J. Vijay, D. P. Selvaraj, P. Ramkumar, IOP Conference Series: Materials Science and Engineering, 247 (2017) 012011. https://doi.org/10.1088/1757-899X/247/1/012011
[11] A. Boutouta, M. Y. Debili, High Temperature Material Processes, 22 (2018). https://doi.org/10.1615/HighTempMatProc.2018027463
[12] L. Singh, S. Sehgal, K. K. Saxena, E3S Web of Conferences, 309 (2021) 01028. https://doi.org/10.1051/e3sconf/202130901028
[13] M. Ravikumar, H. N. Reddappa, R. Suresh, E. R. Babu, C. R. Nagaraja, Frattura ed Integrità Strutturale, 58 (2021) 166. https://doi.org/10.3221/IGF-ESIS.58.12
[14] R. Suresh, M. Ravikumar, H. N. Reddy, E. R. Babu, C. R. Nagaraja, Advances in Materials and Processing Technologies (2022). https://doi.org/10.1080/2374068X.2022.2036583
[15] A. R. J. Katae, H. H. Hussein, A. S. Jaber, M. A. Sarhan, M. RASHEED, Experimental and Theoretical NANOTECHNOLOGY, 10 (2026) 725. https://doi.org/10.56053/10.2.725
[16] R. Zhang, R. Xue, Y. Li, Materials Research Express, 11 (2024) 095508. https://doi.org/10.1088/2053-1591/ad7cca
[17] H. A. S. Aljaafari, S. B. Ali, M. A. Abbas, H. B. Ali, R. A. Anaee, S. A. Naser, R. I. Mahdi, M. A. Anaee, Journal of Bio- and Tribo-Corrosion, 10 (2024) 100. https://doi.org/10.1007/s40735-024-

00902-9
[18] H. A. Abdulaah, A. M. Al-Ghaban, R. A. Anaee, A. A. Khadom, M. M. Kadhim, Journal of Electrochemical Science and Engineering, 13 (2023) 115. https://doi.org/10.5599/jese.1554
[19] S. A. Maged, R. Anaee, M. T. Mathew, International Journal of Corrosion and Scale Inhibition, 12 (2023) 275. https://doi.org/10.17675/2305-6894-2023-12-1-16
[20] M. M. Abbas, A. K. Jassim, L. K. Abbas, Experimental and Theoretical NANOTECHNOLOGY, 9 (2025) 297. https://doi.org/10.56053/9.S.297
[21] B. Klause, G. Bremene, V. Hernn, A. Bosch, Experimental and Theoretical NANOTECHNOLOGY, 3 (2019) 213. https://doi.org/10.56053/3.2.213
[22] G. E. Alkinani, A. R. J. Katae, M. RASHEED, Experimental and Theoretical NANOTECHNOLOGY, 10 (2026) 1027. https://doi.org/10.56053/10.S.1027
[23] N. A. Hikmat, A. M. Farhan, R. A. Anaee, Engineering and Technology Journal, 27 (2009) 1532. https://doi.org/10.30684/etj.27.8.9
[24] Nadia Farid Hassan Sabri, Jassim Muhsin Nasser, Experimental and Theoretical NANOTECHNOLOGY, 10 (2026) 835 https://doi.org/10.56053/10.S.835
[25] Z. S. Aziz, R. A. Anaee, M. H. Abd, S. A. Naser, AIP Conference Proceedings, 2475 (2023) 040016. https://doi.org/10.1063/5.0104435
[26] R. A. Anaee, M. A. Abbas, S. A. Abdul Maged, S. A. Naser, S. S. Hamdi, H. M. Yousif, N. J. Al-Bahnam, T. A. Anai, Experimental and Theoretical NANOTECHNOLOGY, 9 (2025) 449. https://doi.org/10.56053/9.S.449
[27] R. A. Anaee, M. Mahdi, H. A. Al-Kaisy, S. A. Abdul Maged, Engineering and Technology Journal, 32 (2014) 354. https://doi.org/10.30684/etj.32.2A.6
[28] R. A. Anaee, M. H. Abdulmajeed, S. I. Ibrahem, S. A. Abdul Maged, Z. S. Al-Saffar, Engineering and Technology Journal, 32 (2014) 1380. https://doi.org/10.30684/etj.32.6A.3
[29] A. Al-Ghaban, H. Abdullah, R. Anaee, S. Naser, A. Khadom, Journal of Engineering Research, 12 (2024) 299. https://doi.org/10.1016/j.jer.2023.11.020
[30] M. Sayyed, K. Kaky, R. Anaee, Journal of Theoretical and Applied Physics, 18 (2024). https://doi.org/10.1007/s40094-024-00634-2
[31] A. F. Al-Attar, H. A. Jaber, R. A. Anaee, Results in Engineering, 19 (2023) 101327. https://doi.org/10.1016/j.rineng.2023.101327
[32] Y. H. Al-Mawlah, Y. F. Alasadi, M. N. Al-Darraji, Gene Reports, 25 (2021) 101401. https://doi.org/10.1016/j.genrep.2021.101401
[33] A. B. Radhi, S. M. Shartooh, and E. A. Al-Heety, Iraqi Journal of Science, 1 (2021) 1816. https://doi.org/10.24996/ijs.2021.62.6.7
[34] O. Y. M. Alabdali, A. Guessab, Applied Mathematics and Computation, 247 (2014) 1129. https://doi.org/10.1016/j.amc.2014.09.00
[35] O. Alabdali, A. Guessab, Filomat, 34 (2020) 601. https://doi.org/10.2298/FIL2002601A
[36] M. Rasheed, O. Y. Mohammed, S. Shihab, A. Al-Adili, Journal of Physics: Conference Series, 1795 (2021) 012042. https://doi.org/10.1088/1742-6596/1795/1/012042
[37] M. Enneffati, B. Louati, K. Guidara, M. Rasheed, R. Barillé, Journal of Materials Science: Materials in Electronics, 29 (2018) 171. https://doi.org/10.1007/s10854-017-7901-7
[38] A. J. Hussein, M. N. Al-Darraji, M. Rasheed, M. A. Sarhan, IOP Conference Series: Earth and Environmental Science, 1262 (2023) 022005. https://doi.org/10.1088/1755-1315/1262/2/022005
[39] M. Enneffati, M. Rasheed, B. Louati, K. Guidara, R. Barillé, Optical and Quantum Electronics, 51 (2019) 1. https://doi.org/10.1007/s11082-019-2015-5
[40] A. A. Abdulrahman, M. Rasheed, S. Shihab, Journal of Physics: Conference Series, 1879 (2021) 022118. https://doi.org/10.1088/1742-6596/1879/2/022118

[41] F. Dkhilalli, S. Megdiche, K. Guidara, M. Rasheed, R. Barillé, M. Megdiche, Ionics, 24 (2018) 169. https://doi.org/10.1007/s11581-017-2193-8
[42] H. K. Aity, E. Dhahri, M. Rasheed, Ceramics International, 50 (2024) 54666. https://doi.org/10.1016/j.ceramint.2024.10.324
[43] T. Saidani, M. Rasheed, I. Alshalal, A. A. Rashed, M. A. Sarhan, R. Barillé, Research on Engineering Structures and Materials, 9 (2023) 1. https://doi.org/10.17515/resm2023.21ma0922rs